

Supporting information for

X-ray Micro-Computed Tomography for Structural Analysis of All-Solid-State Battery at Pouch Cell Level

*Chen-Jui Huang,^{†,‡} Jin An Sam Oh,^{¶,+} Marta Vicencio,[¶] Tianchen Hu,^{||} Hedi Yang,[†] James N. Burrow,^{†,‡}
Yen-Fang Song,[§] Gung-Chian Yin,[§] Pavel Shevchenko,[‡] Kamila M. Wiaderek,^{‡,±} Bing Joe Hwang,^{⊥,§}
and Ying Shirley Meng^{*,†,¶,±}*

[†]Pritzker School of Molecular Engineering, University of Chicago, Chicago, IL 60637, USA

[‡]Advanced Photon Source, Argonne National Laboratory, Lemont, IL 60439, USA

[¶]Aiiso Yufeng Li Family Department of NanoEngineering, University of California San Diego, La Jolla, CA 92093, United States.

^{||}Argonne National Laboratory, Lemont, IL 60439, USA

[±]Energy Storage Research Alliance, Argonne National Laboratory, Lemont, IL 60439, USA

[§]National Synchrotron Radiation Research Center, Hsinchu, 30076, Taiwan

[⊥]Sustainable Electrochemical Energy Development (SEED) Center, National Taiwan University of Science and Technology, Taipei, 10607, Taiwan

⁺Present address: Jin An Sam Oh, Institute of Materials Research and Engineering (IMRE), Agency for Science, Technology and Research (A*STAR), Singapore 138634, Singapore

Corresponding Author

* Ying Shirley Meng, E-mail: shirleymeng@uchicago.edu and shirleymeng@anl.gov

EXPERIMENTAL METHODS

Materials

$\text{Li}_6\text{PS}_5\text{Cl}$ (LPSCl, NEI Corporation, USA) sulfide-based solid-state electrolyte (SSE) was used as received for the dry-processed separator and composite cathode electrode fabrication. $\text{LiNi}_{0.8}\text{Mn}_{0.1}\text{Co}_{0.1}\text{O}_2$ (NMC811, LG Energy Solution) with a boron-based surface coating layer was used as received for the dry-processed composite cathode electrode. LPSCl powder was mixed with polytetrafluoroethylene (PTFE, Chemours) in a weight ratio of 100:0.1 (LPSCl: VGCF) to fabricate dry-process SSE separators. For dry-processed composite cathode electrodes, NMC811, LPSCl, vapor-grown carbon fiber (VGCF, Sigma-Aldrich), and PTFE were mixed in a weight ratio of 66:31:3:0.5 (NMC811: LPSCl: VGCF: PTFE). Dry process for fabricating the separator and cathode electrode was carried out by mixing the powder without PTFE using a mortar and pestle to obtain a well-mixed powder mixer following the same procedures as reported in our previous work¹. PTFE powder was then added with continuous grinding until the dough-like texture was obtained. The mixed dough was further fibrillated using a vertical hot roller (Xiamen TMAX Battery Equipments Limited) to apply shear force. Finally, the dry-processed LPSCl separator and NMC811 composite cathode electrode films were thinned down to 300 μm and 150 μm , respectively. The $\mu\text{-Si}$ anode electrode was wet-casted following the same procedure as reported in our previous work². The slurry of the $\mu\text{-Si}$ anode electrode was made using a Thinky mixer (ARM-310, Thinky) to disperse 99.9 wt% of $\mu\text{-Si}$ (1-5 μm , Fisher Scientific) and 0.1 wt% of Polyvinylidene fluoride (PVDF, Kynar) in N-Methyl-2-

Pyrrolidone (NMP). The as-prepared slurry was cast onto a Cu foil (12 μm , MTI) using a casting coater and a film applicator. The casted $\mu\text{-Si}$ electrode was vacuum-dried at 80°C overnight to remove the NMP solvent thoroughly.

Pouch cell assembly

The fabricated dry electrolyte separator film, composite cathode electrode film, and wet-casted $\mu\text{-Si}$ anode electrode were punched into 20mm \times 50 mm, 15mm \times 35mm, and 18mm \times 40mm, respectively³. The areal loading of composite cathode electrode is 4.0 mAh cm⁻², pairing with $\mu\text{-Si}$ anode with an N/P ratio of 1.2. To assemble the ASSB pouch cell, $\mu\text{-Si}$ anode, LPSCl separator, NMC811 composite cathode, and Al foil current collector were stacked in sequence. The fabricated cell stack was then welded with Ni and Al tabs onto the Cu and Al current collector terminals, respectively. Finally, the cell was vacuum sealed in an Al-laminated pouch bag and pressurized at 500 MPa by the CIP (YLJ-100E, MTI). All the assembly processes were carried out inside an Ar-filled glovebox (O_2 , H_2O < 1 ppm); only the isostatic press step was performed outside the glovebox under ambient atmosphere.

Pouch cell C-Rate test cycling

The as-assembled ASSB NMC811|LPSCl| $\mu\text{-Si}$ pouch cell was placed inside a customized CIP cycling holder reported in our previous work³. The cycling stack pressure was applied isostatically through compressed air at 5 MPa throughout the C-Rate cycling test at 30°C. Due to the lower Li diffusivity of pure Si before its lithiation, the first activation cycle was conducted by first charging at 0.05C for 5 hours (1C = 200 mA g⁻¹/ 4.0 mA cm⁻²). After the Li diffusivity is improved once the Si is partially

lithiated, the subsequent cycle is cycled at 0.1C. C-Rate test was conducted by cycling the ASSB pouch cell 3 cycles each at 0.1C, 0.2C, 0.3C, 0.4C, 0.5C, 0.7C, 1C, and back to 0.1C, respectively.

3D Focused Ion Beam-Scanning Electron Microscopy

The CIP pressurized composite cathode electrode and separator were attached to a stub and transferred from the glovebox to the scanning electron microscopy (SEM) using the QuickLoader to ensure minimum air exposure. The cross-section is prepared by focused Ga⁺-ion beam milling, and SEM images were obtained using an FEI Scios DualBeam Focused ion beam scanning electron microscope equipped with an Everhart–Thornley Detector. The 3D composite cathode model was obtained by milling 200 nm per slice for 10 μm using the AutoSlice software with a total of 51 slices.

Synchrotron X-ray computed tomography

Synchrotron X-ray computed tomography experiments were conducted at TPS31A Projection X-ray microscopy (PXM) and Transmission X-ray Microscopy (TXM) beamline in Taiwan Photon Source (TPS) at the National Synchrotron Radiation Research Center (NSRRC) at Hsinchu, Taiwan. The energy of X-ray from synchrotron radiation was centered at 40 keV by tuning a double multilayer monochromator (DMM) to conduct 3-dimensional (3D) tomography of the samples. Two sets of objective lenses were used in this work. The field of view and pixel size were 0.83 mm × 0.7 mm and 0.65 μm when using a 20× objective lens, respectively. The field of view and pixel size were 1.7 mm × 1.4 mm and 1.3 μm when adopting a 10× objective lens, respectively. The overhanging edge of the cell was imaged using X-ray energy at 20 keV and a 5× objective lens, with a field of view and pixel size of 3.3 mm × 2.8 mm and 2.6 μm, respectively. The pixel number of the image detector is

2560×2160. The tomography scan was executed by rotating the pouch cell sample azimuthally with a 0.25° interval through ±90° range for 721 projections. Then, all 2D frames were reconstructed as a 3D tomography through an in-house developed software using a filtered-back-projection algorithm. Finally, 3D tomography visualization, segmentation, and analysis were carried out using the Avizo software (Thermo Fisher Scientific Inc.).

Image segmentation workflow

The reconstructed sXCT 3D models of the ASSB pouch cell stack were first cropped into individual components—composite cathode, LPSCl separator, and Si anode on Cu foil—prior to segmentation. Segmentation was conducted using a combination of grayscale thresholding and top-hat techniques in Avizo. The composite cathode was segmented into three phases: active material (NMC811), SSE, and the pore with carbon binder domain (CBD). Thresholding was based on the full width at half maximum (FWHM, 50% contrast) to define the boundaries of each phase. The top-hat tool, configured with a cube kernel shape (neighborhood of 26 and kernel size of 3), was used to better capture the pore/CBD phase, given the geometry of pores. To refine the segmentation, individual connected regions smaller than 3 voxels were removed from each plane (xy, yz, and xz). Regions entirely surrounded by neighbors were integrated, while islands sharing more than 25% of their perimeter with a neighboring region were merged with the surrounding phase.

Visual comparison between FIB-SEM and sXCT images

Figure S1a and **S1b** show a cross-section SEM image and sXCT slice (imaged using a 20× lens) of the dry-process composite NMC811 cathode electrode for comparison, respectively. In both images, NMC811 particles show a brighter contrast compared to LPSCl SSE particles, and the dark regions show the pores and gaps between the NMC811 and LPSCl particles with carbon additive (vapor-grown carbon fiber, VGCF) within. Both images show a similar microstructure of the composite cathode electrode. However, SEM shows a spatial resolution of ~ 15 nm with an imaging size of $26 \times 35 \mu\text{m}^2$, while sXCT shows a pixel size of $\sim 0.65 \mu\text{m}$ with a larger imaging size of $122 \times 166 \mu\text{m}^2$, nearly half an order of magnitude.

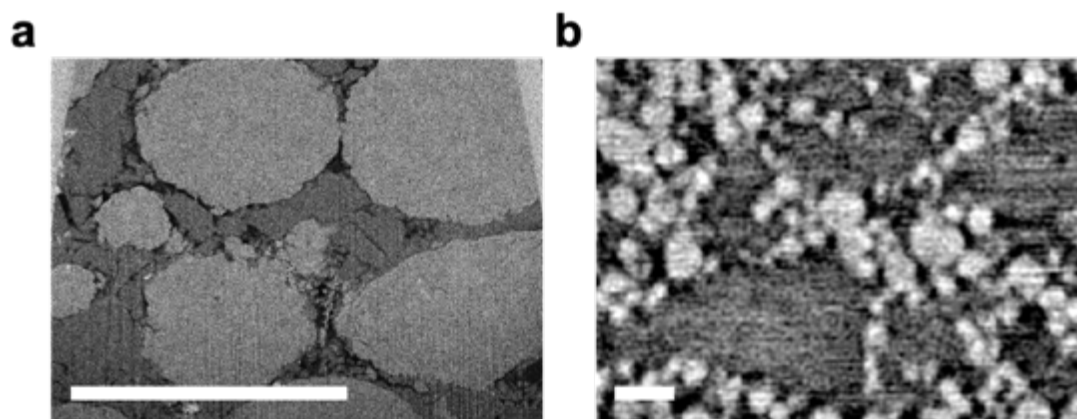


Figure S1. Comparison between FIB-SEM and sXCT images. (a) Cross-section FIB-SEM image and (b) Cross-section micro-CT slice of composite cathode. Scale bar: 20 μm .

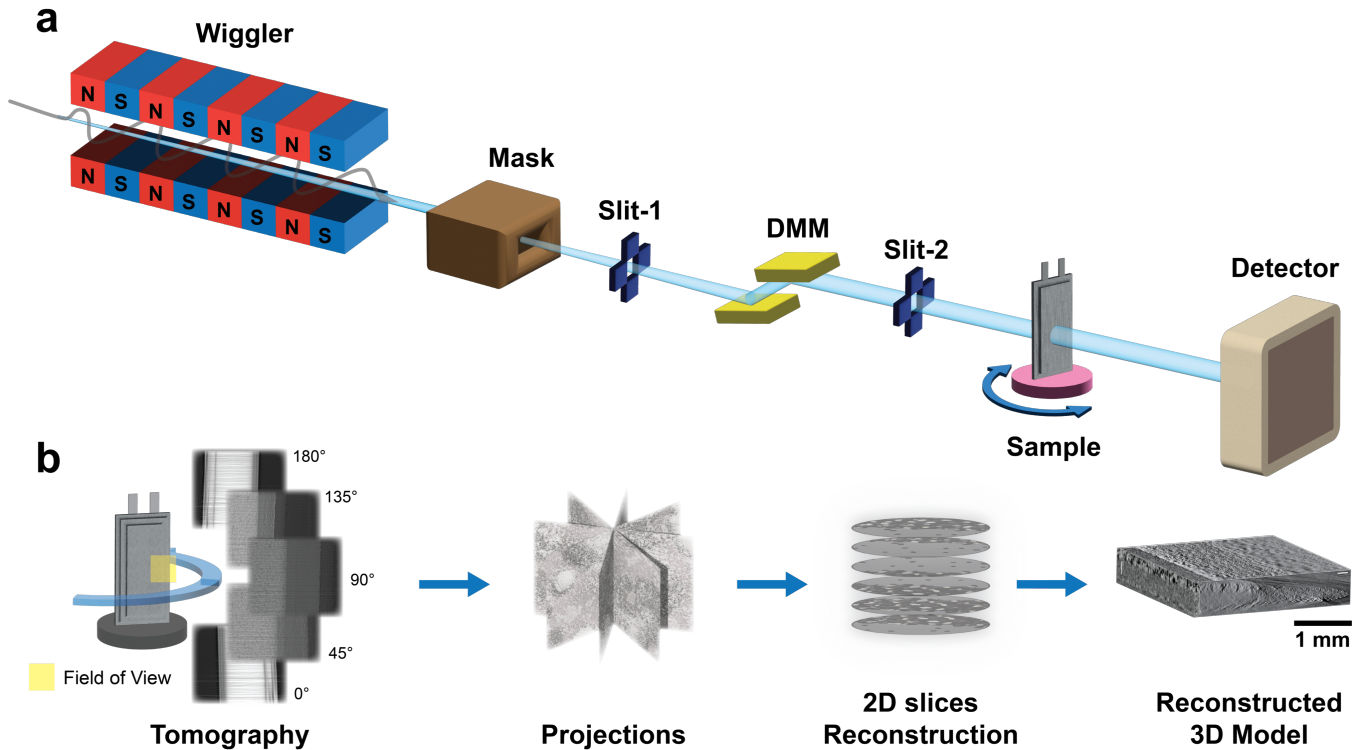


Figure S2. Schematic of synchrotron X-ray micro-CT experiments. (a). Schematic of synchrotron-based micro-CT beamline using double multilayer monochromators (DMM) mode. (b). sXCT tomography and reconstruction workflow.

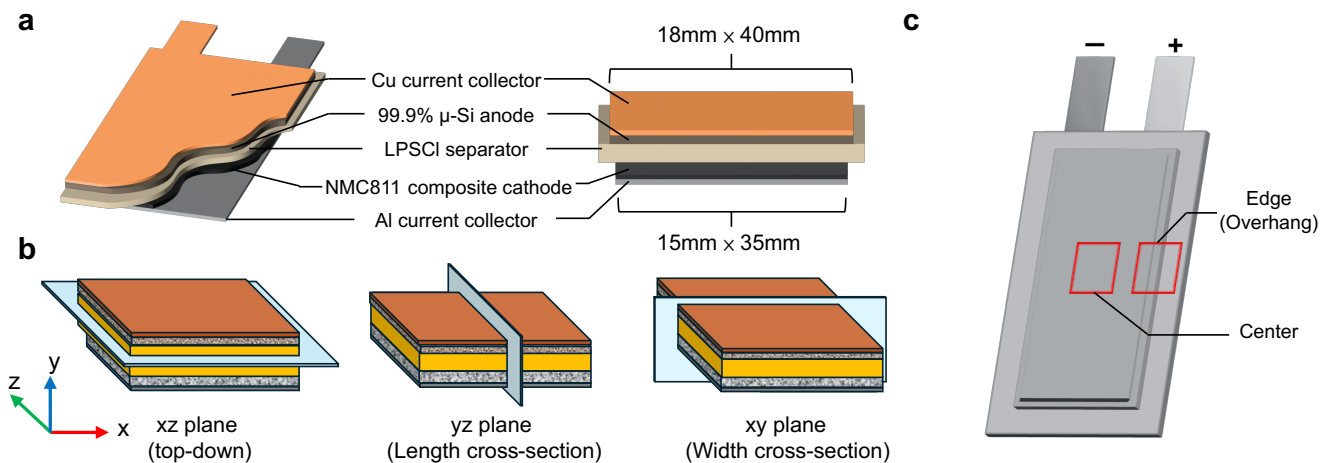


Figure S3. Cell configuration of ASSB pouch cell and sXCT slice perspectives. (a) Schematic of ASSB pouch cell configuration and dimension. (b) Three perspectives of sXCT slices for visualizing

xz, yz, and xy planes. The light blue plane indicates the visualizing section of sXCT image. (c) Schematic showing the sXCT imaged region of pouch cells.

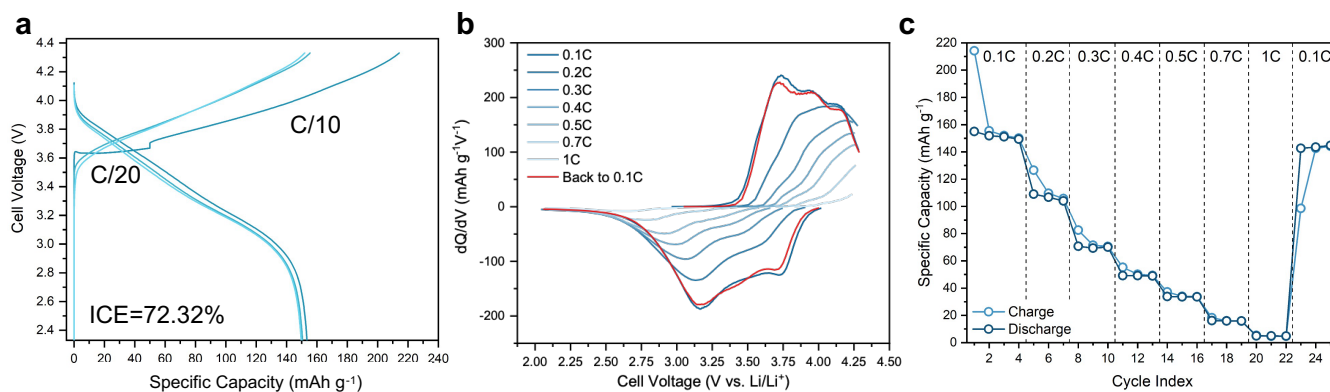


Figure S4. Electrochemical performance of ASSB pouch cell. (a) First three cycles of ASSB pouch cell that was used for CT experiments. (b) dQ/dV analysis showing the last cycle of each C-rate of the C-rate test. (c) C-rate test of the ASSB pouch cell used for CT experiments. In the first cycle, the cell was charged at C/20 for the first 5 hours before changing to C/10. The cycling stack pressure is 5 MPa under an isostatic environment. (1C = 200 mA g⁻¹)

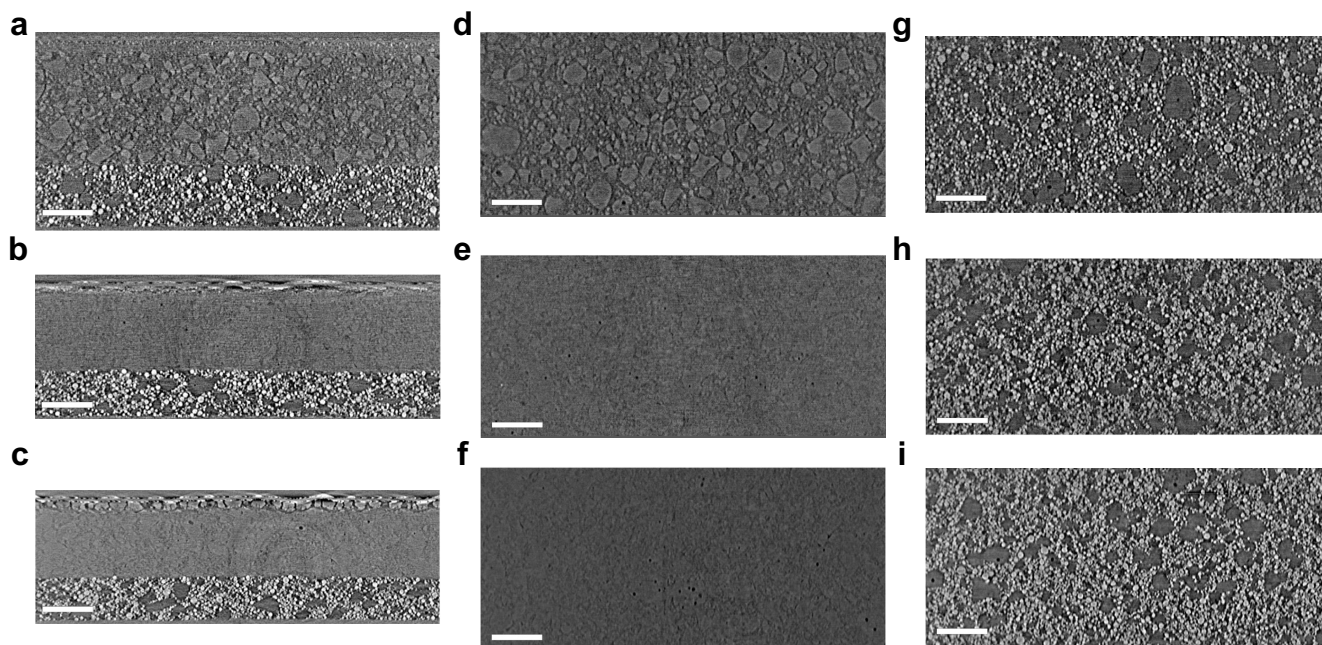


Figure S5. Cross-section micro-CT slice of ASSB pouch cell. The cross-section xy slices of the entire cell stack of the (a) assembled, (b) pressed, and (c) cycled pouch cells. The top-down xz slice of separator and cathode composite of the (d,g) assembled, (e,h) pressed, and (f,i) cycled pouch cells, respectively. Scale bar: 150 μm .

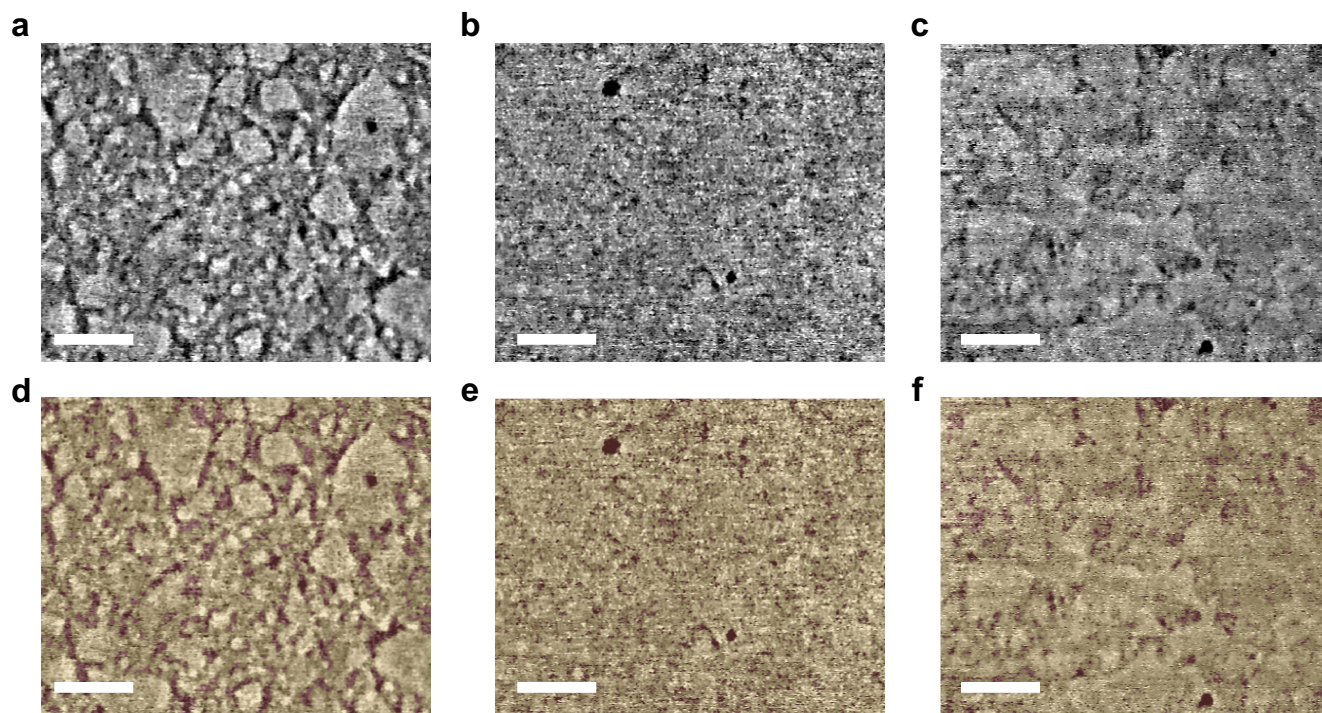


Figure S6. Segmentation of LPSCI separator layer. The xz slice of SSE separator layer of the (a) assembled, (b) pressed, and (c) cycled pouch cells. The color-wash xz slice of segmented SSE separator of the (d) assembled, (e) pressed, and (f) cycled pouch cells. Scale bar: 50 μm .

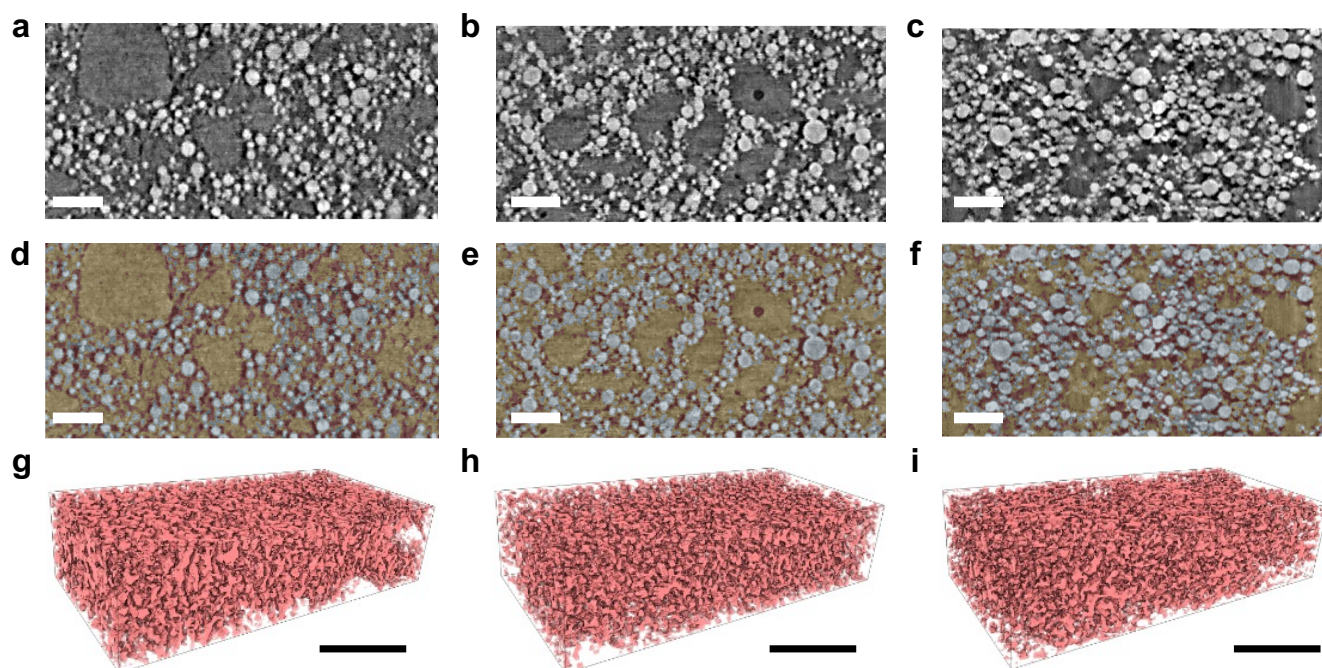


Figure S7. Overlay of segmentation results with x-ray CT slice cathode composite layer. The xz slice of composite cathode layer of the (a) assembled, (b) pressed, and (c) cycled pouch cells. Scale bar: 50 μm . The color-wash xz slice of the segmented cathode composite layer of the (d) assembled, (e) pressed, and (f) cycled pouch cells. Scale bar: 50 μm . The 3D model of pores/VGCF of the (g) assembled, (h) pressed, and (i) cycled pouch cells. Scale bar: 100 μm .

sXCT segmentation validation

To validate the tomography and segmentation results obtained from the sXCT data, a 3D FIB-SEM experiment was performed on the same CIP-pressurized composite cathode film. **Figure S8a** displays the FIB-SEM cross-sectional image of the composite cathode (field of view: $21.8 \times 30.2 \mu\text{m}^2$), while **Figure S8b** shows the segmentation results with color-washed components. The $\text{LiNi}_{0.8}\text{Mn}_{0.1}\text{Co}_{0.1}\text{O}_2$ (NMC811), $\text{Li}_6\text{PS}_5\text{Cl}$ (LPSCl), and pores/ carbon binder domain (CBD) are labeled in blue, yellow, and pink, respectively. The 3D model of pores/CBD is shown in **Figure S8c**. The volume fractions obtained from the FIB-SEM segmentation are 41.2:49.3:9.5 (NMC811: LPSCl: pore/CBD), which are in close agreement with the sXCT-derived values of 36.3:49.8:13.9. The slight variations in NMC811 and pores/carbon fractions may arise from the localized field of view in the FIB-SEM measurement, which may not fully represent the bulk volume fraction.

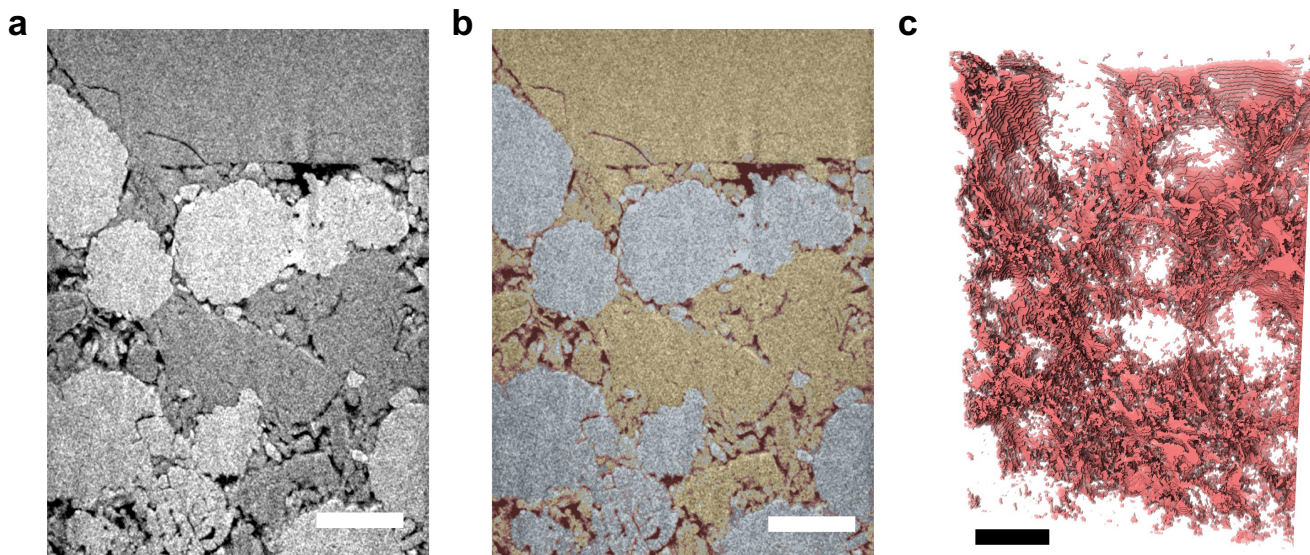


Figure S8. 3D FIB-SEM model and segmentation validation (a) FIB slice of pressed composite cathode. (b) Color wash FIB slice indicating the segmentation results for the 3D FIB-SEM reconstructed model. (c) The 3D model of pores in the CIP-pressed composite cathode obtained from 3D FIB-SEM. Scale bar: 5 μm .

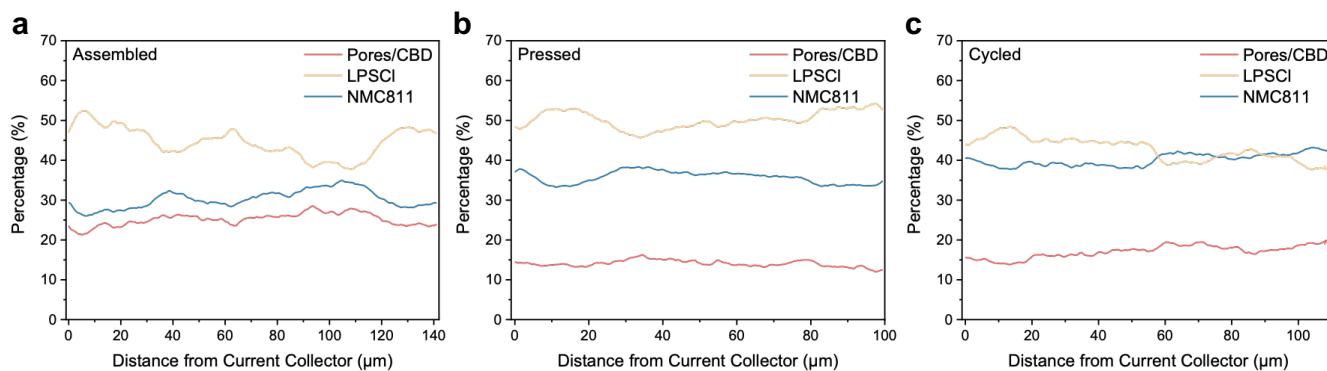


Figure S9. Volume fraction of composite cathode across the thickness. Volume fraction of each component in composite cathode in the (a) assembled, (b) pressed, and (c) cycled pouch cells, respectively.

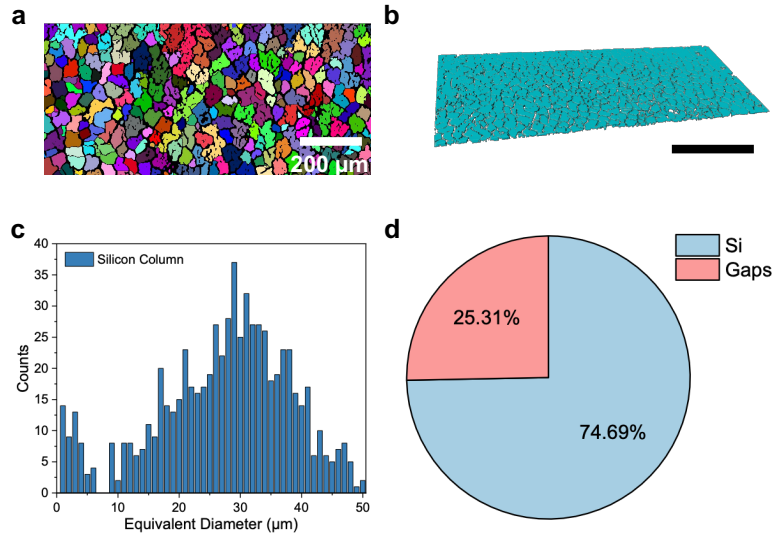


Figure S10. Segmentation detail for Si anode. (a) The xz-slice of segmented results for individual Si columns. Scale bar: 200 μm . 3D models of cycled pouch cell showing the (b) segmented Si columns. Scale bar: 400 μm . (c) Equivalent diameter distribution of Si columns obtained from segmentation and labeling result. (d) Area fraction of Si columnar structure and mud cracks based on the segmented xz slice.

REFERENCES

- (1) Lee, D. J.; Jang, J.; Lee, J. P.; Wu, J.; Chen, Y. T.; Holoubek, J.; Yu, K.; Ham, S. Y.; Jeon, Y.; Kim, T. H.; et al. Physio-Electrochemically Durable Dry-Processed Solid-State Electrolyte Films for All-Solid-State Batteries. *Advanced Functional Materials* **2023**, *33* (28), 2301341. DOI: 10.1002/adfm.202301341
- (2) Tan, D. H. S.; Chen, Y. T.; Yang, H.; Bao, W.; Sreenarayanan, B.; Doux, J. M.; Li, W.; Lu, B.; Ham, S. Y.; Sayahpour, B.; et al. Carbon-free high-loading silicon anodes enabled by sulfide solid electrolytes. *Science* **2021**, *373* (6562), 1494-1499. DOI: 10.1126/science.abg7217
- (3) Chen, Y. T.; Jang, J.; Oh, J. A. S.; Ham, S. Y.; Yang, H.; Lee, D. J.; Vicencio, M.; Lee, J. B.; Tan, D. H. S.; Chouchane, M.; et al. Enabling Uniform and Accurate Control of Cycling Pressure for All-Solid-State Batteries. *Advanced Energy Materials* **2024**, *14* (30), 2304327. DOI: 10.1002/aenm.202304327